

## Silicate polymerization on crystalline and amorphous TiO<sub>2</sub>: an ATR-IR and synchrotron XPS investigation

YANTAO SONG<sup>1\*</sup>, PETER JAMES SWEDLUND<sup>1</sup>, JAMES METSON<sup>1</sup>, GEOFFREY I.N. WATERHOUSE<sup>1</sup> AND BRUCE COWIE<sup>2</sup>

<sup>1</sup>School of Chemical Sciences, the University of Auckland, y.song@auckland.ac.nz (\* presenting author)

<sup>2</sup>Australian Synchrotron, SoftXRay@synchrotron.org.au

### Introduction

The presence of silicate at metal oxide-aqueous interfaces influences many oxide properties. Understanding the chemistry of silicate at these interfaces is important to describe the geochemistry of these metal oxides and elements associated with the oxides [1-2]. This work compares silicate sorption and polymerization on the disordered surface of an amorphous TiO<sub>2</sub> (TiO<sub>2(am)</sub>) with silicate chemistry on the well defined faces of rutile TiO<sub>2</sub>. The work used *in situ* attenuated total reflectance-infrared spectroscopy (ATR-IR) and *ex situ* synchrotron based X-ray photoelectron spectroscopy (XPS).

### Results and Conclusion

The ATR-IR results show that a monomeric silicate species with a Si-O stretching mode at  $\approx 950$  cm<sup>-1</sup> formed on all TiO<sub>2</sub> surfaces at low surface coverage. Linear oligomeric silicates with a Si-O IR adsorbance at  $\approx 1020$  cm<sup>-1</sup> form when the surface coverage reaches a threshold value (Figure 1). The process of silicate oligomerization was favoured on the crystalline rutile surface compared to the amorphous TiO<sub>2</sub>. This agrees with the XPS results and the proposed model of heterogeneous silicate polymerization which would be favoured by the arrangement of TiO<sub>2</sub> octahedra on the rutile (110) face (Figure 2).

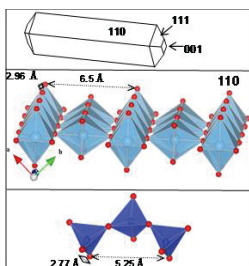
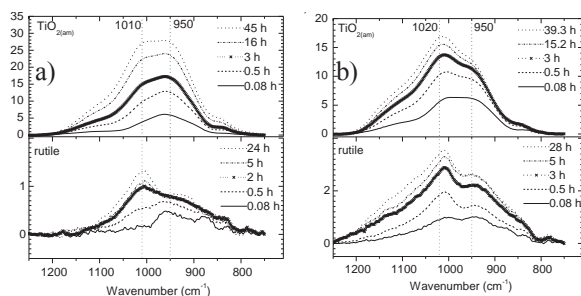


**Figure 1 (above):** ATR-IR spectra of H<sub>4</sub>SiO<sub>4</sub> adsorbed on the surface of TiO<sub>2(am)</sub> and rutile at pH 9 and 0.1 M NaCl measured over time. Final concentrations of H<sub>4</sub>SiO<sub>4</sub> are (a) 0.2 mM and (b) 1.5 mM.

**Figure 2 (left):** Rutile morphology and enclosing faces. Bottom panel shows a section of ferrosilite, a linear silicate.

[1] Swedlund *et al.* (2011) *Chem. Geol.* **285**, 62-69.

[2] Dol Hamid *et al.* (2011) *Langmuir.* **27**, 12930-12937.

## Cr(VI) Reduction and Isotopic Fractionation In Bacteria: Cytoplasmic/Extracellular Reduction Rate and Diffusion Controls

ERIC SONNENTHAL<sup>1\*</sup>, JOHN N. CHRISTENSEN<sup>1</sup>, AND RUYANG HAN<sup>1</sup>

<sup>1</sup>Earth Sciences Division, Lawrence Berkeley National Lab, Berkeley, CA, USA, [elsonmenthal@lbl.gov](mailto:elsonmenthal@lbl.gov) (\* presenting author)

Reduction of Cr(VI) to Cr(III) by bacteria is well documented and leads to significant Cr isotopic fractionation (<sup>53</sup>Cr/<sup>52</sup>Cr), with experimental values in abiotic systems of  $\sim 3.4\%$ [1] to  $5\%$ [2], and theoretical equilibrium values of  $6-7\%$ [3]. Biologically-mediated Cr isotopic fractionation of  $\sim 4.2\%$ [4] has been attributed to kinetic fractionation, with possible controls by metabolic pathways, transport, or reduction sites. In lactate-amended cell suspension experiments with *Pseudomonas stutzeri* strain RCH2, Cr isotopic fractionation was less under denitrifying vs. aerobic conditions[5], and attributed to Cr(VI) transport limitation. In this work, a reactive-transport model was developed to evaluate effects of cytoplasmic/extracellular reduction rates and transport in bacteria on Cr isotopic fractionation with comparison to experimental data.

The multicontinuum reactive-transport model is based on a simplified structure of bacterium *Pseudomonas stutzeri*, of average dimension of  $2 \times 0.5 \mu\text{m}$ , a cell membrane thickness of 15nm, and an average bacterium spacing derived from the suspension cell density. Cr reduction in the cytoplasm is dependent on chromate diffusive transport through the outer membrane (via sulfate channels), the periplasmic space, and to reduction sites. Cell wall diffusivities were estimated from published cell wall permeabilities. Cr reduction was assumed to be thermodynamically and kinetically-controlled by Cr(OH)<sub>3</sub> precipitation using a solid solution model of <sup>53</sup>Cr(OH)<sub>3</sub> and <sup>52</sup>Cr(OH)<sub>3</sub>. Simulations considered an aerobic case with lactate oxidation to pyruvate, and a denitrifying case forming pyruvate, as well as conditions of the experiments described in [4].

Simulations with differing cell densities using Toughreact [7] showed that it is necessary to limit diffusive transport through the cell wall by  $\sim 4$  orders of magnitude to match the change in Cr isotopic fractionation from  $\sim 2\%$  (aerobic) to  $\sim 0.4\%$  (denitrifying). By severely limiting diffusive transport, Cr reduction rates decrease significantly, inconsistent with experimental data. In contrast, by increasing the Cr reduction rate in the cytoplasm, a large decrease in the fractionation factor is observed, without inhibiting the Cr reduction rate, capturing the observed <sup>53</sup>Cr/<sup>52</sup>Cr and Cr reduction rates over a range of cell densities. Although it is not known where Cr reduction was localized in the cell suspension experiments[5], simulations show that Cr reduction in the extracellular medium also leads to higher Cr reduction rates and Cr isotopic ratios close to the maximum value for the reduction reaction.

[1] Ellis, Johnson & Bullen (2002) *Science* **295**, 2060-2062. [2] Zink, Schoenberg & Staubwasser (2010) *GCA* **74**, 5729-5745. [3] Schauble, Rossman & Taylor (2004) *Chem Geol* **205**, 99-114. [4] Sikora, Johnson & Bullen (2008) *GCA* **72**, 3631-3641. [5] Han *et al.* (in press) *AEM*. [6] Han *et al.* (2010) *ES&T* **44**, 7491-7497. [7] Xu *et al.* (2011) *Comp Geosc* **37**, 763-774.